Bull Earthquake Eng
DOI 10.1007/s10518-016-0052-z

ORIGINAL RESEARCH PAPER

Experimental evaluation of four ground-motion scaling methods for dynamic response-history analysis of nonlinear structures

Andrew P. O'Donnell[1] · Yahya C. Kurama[2] · Erol Kalkan[3] · Alexandros A. Taflanidis[2]

Received: 18 February 2016 / Accepted: 18 November 2016

Abstract This paper experimentally evaluates four methods to scale earthquake ground-motions within an ensemble of records to minimize the statistical dispersion and maximize the accuracy in the dynamic peak roof drift demand and peak inter-story drift demand estimates from response-history analyses of nonlinear building structures. The scaling methods that are investigated are based on: (1) ASCE/SEI 7–10 guidelines; (2) spectral acceleration at the fundamental (first mode) period of the structure, $S_a(T_1)$; (3) maximum incremental velocity, *MIV*; and (4) modal pushover analysis. A total of 720 shake-table tests of four small-scale nonlinear building frame specimens with different static and dynamic characteristics are conducted. The peak displacement demands from full suites of 36 near-fault ground-motion records as well as from smaller "unbiased" and "biased" design subsets (bins) of ground-motions are included. Out of the four scaling methods, ground-motions scaled to the median *MIV* of the ensemble resulted in the smallest dispersion in the peak roof and inter-story drift demands. Scaling based on *MIV* also provided the most accurate median demands as compared with the "benchmark" demands for structures with greater nonlinearity; however, this accuracy was reduced for structures exhibiting reduced nonlinearity. The modal pushover-based scaling (MPS) procedure was the only method to conservatively overestimate the median drift demands.

Keywords Ground-motion scaling · Maximum incremental velocity · Modal pushover-based scaling · Nonlinear dynamic response-history analysis · Shake-table testing

✉ Yahya C. Kurama
ykurama@nd.edu

[1] AIR Worldwide, 131 Dartmouth St, Boston, MA 02116, USA

[2] Civil and Environmental Engineering and Earth Sciences, University of Notre Dame, Notre Dame, IN 46556, USA

[3] Earthquake Science Center, United States Geological Survey, Menlo Park, CA 94025, USA

Published online: 02 December 2016

1 Introduction

Linear or nonlinear dynamic response-history analysis (RHA) procedures for performance-based seismic design and assessment require selection and scaling of earthquake ground acceleration time-histories that are compatible with the site-specific hazard level(s) considered (e.g., Design Basis Earthquake; Maximum Considered Earthquake). Current building codes and design standards provide limited and unspecific guidance for performing this task, which has the potential to result in different scaling factors, and subsequently, different engineering demand estimates from the dynamic analyses (Kalkan and Chopra 2009). For example, consider the seismic design of a structure based on the Nonlinear Seismic Response History Procedure in ASCE/SEI 7–10 (2010) (abbreviated henceforth as ASCE 7). In determining the engineering demands (e.g., inter-story drift) used in design, ASCE 7 mandates that either the maximum demands from nonlinear RHAs over a minimum of three records or the average (arithmetic mean) demands from nonlinear RHAs over a minimum of seven records be used. The procedure in ASCE 7 requires that each ground-motion record used in design be scaled with a factor to minimize the difference between its elastic acceleration response spectrum and the target (design) spectrum over a period range of $0.2T_1$–$1.5T_1$ (where T_1 is the fundamental vibration period of the building).

It has been shown that ground-motion records scaled according to ASCE 7 method can result in significant variability (dispersion) in the dynamic displacement demands of a structure (Kalkan and Chopra 2010a, b, 2012; O'Donnell et al. 2013a; Reyes et al. 2015). A consequence of this large dispersion is that different suites of seven (or three) records scaled per ASCE 7 can result in drastically different average (or maximum, in the case of three records) demands, and therefore, drastically different design outcomes (i.e., over-design, under-design, or satisfactory). To reduce this variability, the scaling method used in design should reduce the level of dispersion in the engineering demands such that when different suites of a relatively small number of records (e.g., three or seven records per ASCE 7) are scaled to the same target intensity level, the design outcome is not greatly affected. Although the use of an increased number of records may improve estimates of the average demands, this approach may not be practical. Furthermore, the use of a large number of records does not answer the question of how these records should be scaled to represent a given seismic hazard level.

Considering these issues, the current paper presents and evaluates the responses from small-scale shake-table experiments of a set of four nonlinear multi-story building frame structures subjected to ground-motion suites scaled using four different methods. The test specimens were designed and constructed to be reusable, thus allowing multiple shake-table tests to be conducted with each test starting from essentially the same initial conditions even after the specimen had exhibited significant nonlinear response from a previous test. Each structure was subjected to one unscaled and four scaled ground-motion suites, with 36 records in each suite, resulting in 720 tests [(4 structures) × (5 suites) × (36 records)]. The paper compares the ground-motion scaling methods with regards to their ability to: (1) provide accurate estimates of the median roof and inter-story drift demands as if a much larger set of records were used; and (2) to minimize the number of records needed to reliably obtain these median demand estimates. Evaluations of peak drift demands from the full suites of 36 ground-motion records as well as from smaller "unbiased" subsets and "biased" subsets (by selecting consistently stronger or weaker records) of ground-motions are included in the investigation.

2 Background and research significance

The topic of ground-motion scaling for RHA has been studied by many researchers (e.g., Nau and Hall 1984; Shome and Cornell 1998; Kurama and Farrow 2003; Naeim et al. 2004; Haselton 2009; Reyes and Chopra 2012; Kalkan and Chopra 2012; Reyes et al. 2015). Shome and Cornell (1998) and Shome et al. (1998) found that when the ground-motion records in an ensemble are scaled so that their linear-elastic spectral response acceleration, $S_a(T_1)$ at the structure fundamental period, T_1 is equal to the median spectral intensity of the ensemble, the dispersion in the demand estimates can be significantly reduced while maintaining similar median demands. Dispersion can be further reduced by scaling at higher levels of damping (Shome and Cornell 1998; Kennedy et al. 1984). However, this scaling method becomes less accurate (i.e., increased error in the median demands) and less efficient (i.e., increased dispersion in the demand estimates) for taller structures with significant higher mode response and for structures responding more into the nonlinear range (Mehanny 1999; Alavi and Krawinkler 2000). Kurama and Farrow (2003) found that for nonlinear structures with a wide range of typical fundamental periods, scaling based on the Maximum Incremental Velocity [*MIV*; defined as the maximum area under the acceleration time-history of a record between two consecutive zero acceleration crossings; see Kurama and Farrow (2003)] is more effective than scaling based on $S_a(T_1)$, especially for structures analyzed under soft soil and/or near-field ground-motion records.

More recently, Kalkan and Chopra (2009) showed that scaling earthquake records based on an equivalent nonlinear single-degree-of-freedom (SDF) representation of the structure produces accurate estimates of the median displacement demands and also reduces the dispersion in the demands. This “modal pushover-based” scaling (MPS) procedure explicitly considers structural strength, determined from the first-mode pushover curve (also referred to as the “capacity” curve, which is often available prior to nonlinear RHA in practice), and determines a scaling factor for each record to match a target value of the displacement of the first-mode equivalent nonlinear SDF model. The SDF displacements are estimated from nonlinear dynamic response history analyses (as was done in this research), or alternatively, using approximate nonlinear displacement demand prediction relationships (e.g., Chopra and Chinatanapakdee 2004). The MPS procedure has been shown to be accurate and efficient for low-, medium-, and high-rise buildings with symmetric plan (Kalkan and Chopra 2010a, b) and ordinary-standard bridges (Kalkan and Kwong 2010, 2012) subjected to one component of ground-motion. However, Ay and Akkar (2014) found that the engineering demands from the MPS procedure may be sensitive to the selected nonlinear displacement demand prediction relationship to determine the equivalent SDF displacements. Reyes and Chopra (2012) extended the MPS procedure from one component of ground-motion to two horizontal components. Lastly, Reyes and Quintero (2013) proposed a new version of the MPS procedure for single-story unsymmetric-plan buildings. This new version was extended to multi-story unsymmetric-plan buildings in Reyes et al. (2015).

While there have been numerous SDF studies on ground-motion scaling, studies based on multi-degree-of-freedom (MDF) systems are more limited. For example, the study by Kurama and Farrow (2003) considered two MDF structures under 20 ground-motion records scaled using two different methods. Similarly, Shome and Cornell (1998) included two MDF models, which were stick-models with 1-DOF per node. The analyses in these studies are dwarfed in number by the current experimental study that includes 720 nonlinear shake-table tests for four MDF structures. Thus, the large number of experiments conducted herein offers extensive and new evidence on the relative performance of the scaling methods chosen. The other primary new contributions of this paper are: (1) comparison of the peak inter-story drift demands in addition to the peak roof drift demands; and (2) evaluation of the demands from unbiased and biased selections of smaller ground-motion subsets (with seven records in each suite) to simulate scenarios that are more typical of design in practice.

The paper builds on a previous experimental study by the authors on the scaling of ground-motion records for linear-elastic structures (O'Donnell et al. 2013a), with the objective of extending the evaluation to nonlinear structures. The previous study demonstrated that the $S_a(T_1)$ scaling method is most effective in minimizing dispersion and maximizing accuracy in the displacement demand estimates for linear-elastic structures. However, inaccuracies in the design estimation of T_1 can significantly erode the effectiveness of the $S_a(T_1)$ method and other period-dependent scaling methods. In the next sections, the ground-motion suites and scaling methods used in the current study are summarized, followed by a description of the test specimens. The results of the experimental program are then presented and extensive comparisons are made between the scaling methods. More information on the motivation for the study, the selected ground-motion records and scaling methods, and the test setup and specimens can be found in O'Donnell et al. (2013a, b, 2015).

3 Ground-motion records and scaling methods

The 36 ground acceleration histories used in the shake-table testing program were from 39 near-fault earthquake ground-motion records. These records, listed in Table 1, were selected from the PEER ground-motion database from seven shallow crustal earthquakes with moment magnitudes in the range of 6.9–7.1, and at distances of 0.2–19.9 km to the causative fault. The ground-motion ensemble consists of impulsive and non-pulse type records in order to cover a wide range of near-fault effects. Such effects include intense seismic demands associated with long-period coherent velocity pulse(s) due to impulsive records as well as cumulative demands associated with large number of cycles due to non-pulse type records (Kalkan and Kunnath 2006).

Using the original 39 records, five suites of ground-motions were produced as follows: (1) GM[Uns]—unscaled suite; (2) GM[ASCE7]—records scaled according to ASCE 7 (2010); (3) GM[$S_a(T_1)$]—records scaled to the median linear-elastic spectral acceleration, $S_a(T_1)$ of the suite at the fundamental period, T_1 of each structure (Shome et al. 1998); (4) GM[MIV]—records scaled to the median *MIV* of the suite (Kurama and Farrow 2003); and (5) GM[MPS]—records scaled based on the modal pushover-based scaling (MPS) procedure (Kalkan and Chopra 2009, 2010a).

As examples, Fig. 1a–e show the 0.78%-damped linear-elastic acceleration response spectra, S_a of the 39 records in the unscaled and scaled suites for one of the test specimens described in this paper (Frame NL4R4), where $\xi = 0.78\%$ is the measured linear-elastic critical damping ratio of all four frame specimens. Each ground-motion record in the GM[MIV] suite was scaled such that its *MIV* was equal to the median [geometric mean; as described in Cornell et al. (2002)] *MIV* of the 39 unscaled records. Similarly, each record in the GM[$S_a(T_1)$] suite was scaled such that its $S_a(T_1)$ was equal to the median $S_a(T_1)$ of the unscaled suite. The $S_a(T_1)$ values were determined from spectra calculated using the

Table 1 Selected near-fault ground-motion records

Record ID	Earthquake name	Station name	Year	M_w	Fault dist. (km)	V_{S30} (m/s)	*PGA* (g)
1058-E	Düzce, Turkey	Lamont 1058	1999	7.1	0.2	425	0.111
1059-N	Düzce, Turkey	Lamont 1059	1999	7.1	4.2	425	0.147
1061-E	Düzce, Turkey	Lamont 1061	1999	7.1	11.5	481	0.134
1062-E	Düzce, Turkey	Lamont 1062	1999	7.1	9.2	338	0.257
375-N	Düzce, Turkey	Lamont 375	1999	7.1	3.9	425	0.970
531-N	Düzce, Turkey	Lamont 531	1999	7.1	8	660	0.159
BOL090	Düzce, Turkey	Bolu	1999	7.1	12	326	0.822
DZC270	Düzce, Turkey	Düzce	1999	7.1	6.7	276	0.535
A-CTR270	**Irpinia, Italy**	**Calitri**	**1980**	**6.9**	**17.6**	**600**	**0.176**
AMA090	Kobe, Japan	Amagasaki	1995	6.9	11.3	256	0.363
FKS090	Kobe, Japan	Fukushima	1995	6.9	17.9	256	0.216
KJM000	Kobe, Japan	KJMA	1995	6.9	1	312	0.821
NIS090	Kobe, Japan	Nishi-Akashi	1995	6.9	7.1	609	0.503
PRI000	**Kobe, Japan**	**Port Island (0 m)**	**1995**	**6.9**	**3.3**	**198**	**0.315**
SHI000	Kobe, Japan	Shin-Osaka	1995	6.9	19.1	256	0.243
TAK090	Kobe, Japan	Takatori	1995	6.9	1.5	256	0.616
TAZ090	Kobe, Japan	Takarazuka	1995	6.9	0.3	312	0.694
BRN090	Loma Prieta, CA	BRAN	1989	6.9	10.7	376	0.501
CAP000	Loma Prieta, CA	Capitola	1989	6.9	15.2	289	0.529
CLS000	Loma Prieta, CA	Corralitos	1989	6.9	3.9	463	0.644
G02000	Loma Prieta, CA	Gilroy Array #2	1989	6.9	11.1	271	0.367
G03000	Loma Prieta, CA	Gilroy Array #3	1989	6.9	12.8	350	0.555
G04000	Loma Prieta, CA	Gilroy Array #4	1989	6.9	14.3	222	0.417
G06090	Loma Prieta, CA	Gilroy Array #6	1989	6.9	18.3	664	0.170
GIL067	Loma Prieta, CA	Gilroy-Gavilan Coll.	1989	6.9	10	730	0.357
GOF160	Loma Prieta, CA	Gilroy-Historic Bldg.	1989	6.9	11	339	0.284
LGP090	Loma Prieta, CA	LGPC	1989	6.9	5	1070	0.605
LOB000	Loma Prieta, CA	UCSC Lick Observatory	1989	6.9	18.4	714	0.450
SJTE225	Loma Prieta, CA	San Jose-Santa Teresa Hills	1989	6.9	14.7	672	0.275
STG000	Loma Prieta, CA	Saratoga-Aloha Ave	1989	6.9	8.5	371	0.512
UC2090	Loma Prieta, CA	UCSC	1989	6.9	18.5	714	0.396
WAH090	Loma Prieta, CA	WAHO	1989	6.9	17.5	376	0.638
WVC270	Loma Prieta, CA	Saratoga-W Valley Coll.	1989	6.9	9.3	371	0.332
CPM000	Cape Mendocino, CA	Cape Mendocino	1992	7.0	7	514	1.497
FOR000	**Cape Mendocino, CA**	**Fortuna–Fortuna Blvd**	**1992**	**7.0**	**19.9**	**457**	**0.116**
PET090	Cape Mendocino, CA	Petrolia	1992	7.0	8.2	713	0.662
RIO360	Cape Mendocino, CA	Rio Dell Overpass-FF	1992	7.0	14.3	312	0.549
HEC090	Hector Mine, CA	Hector	1999	7.1	12	685	0.337
I-ELC180	Imperial Valley-02	El Centro Array #9	1940	6.9	6.1	213	0.313

M_w, moment magnitude; V_{S30}, average shear-wave velocity of surface geology between 0 and 30 m; *PGA*, peak ground acceleration

Records in bold rows (A-CTR270, PRI000, FOR000) were not used in shake-table testing

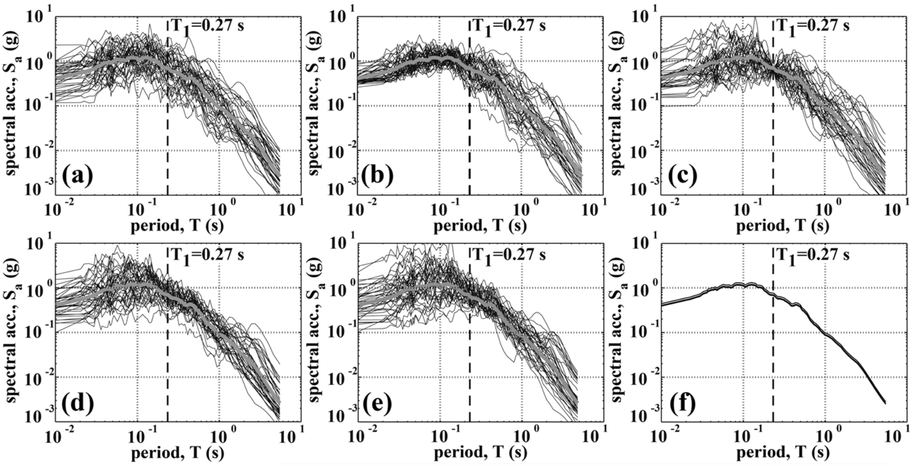

Fig. 1 Linear-elastic S_a spectra ($\xi = 0.78\%$) of the 39 records in the unscaled and scaled suites for Frame NL4R4: **a** GM[Uns]; **b** GM[ASCE7]; **c** GM[$S_a(T_1)$]; **d** GM[MIV]; **e** GM[MPS]; **f** median S_a for all five suites, demonstrating that the median intensities of the different scaled suites were very similar

measured linear-elastic damping ratio of 0.78% for each specimen, which was relatively low. The effects of this damping choice for the $S_a(T_1)$ method are discussed later.

The GM[ASCE7] records were scaled such that the average (arithmetic mean) S_a spectrum for the suite was equal to or greater than the median (geometric mean) spectrum of the unscaled records over the period range between $0.2T_1$ and $1.5T_1$. For the critical damping ratio, $\xi = 5\%$ (instead of the measured ξ) was used in scaling the GM[ASCE7] suite, because this is a specific requirement per ASCE 7. Note that it is possible to determine different sets of scaling factors that satisfy the ASCE 7 scaling requirement. In this research, an optimization algorithm given in Kalkan and Chopra (2010b) was used to determine the scaling factor for each record such that the SRSS (square root of the sum of the squares) error between the average spectrum of the scaled suite and the median spectrum of the unscaled suite was minimized over the period range between $0.2T_1$ and $1.5T_1$.

The GM[MPS] records were scaled by matching the peak displacement demand from the nonlinear response history analysis of the equivalent SDF model for each test structure (determined from the measured pushover load–displacement curve) under each scaled record with the median demand for the same SDF model under the full suite of 39 unscaled records (Kalkan and Chopra 2010a, 2011).

The median response spectra of the five suites of unscaled and scaled records are shown in Fig. 1f, demonstrating that even though each scaling method changed the amplitude of each record, the median intensities of the different scaled suites were very similar. As described in O'Donnell et al. (2013b) and marked in bold in Table 1, three of the 39 scaled records were ultimately excluded from the shake-table tests because of expected demands that exceeded the equipment limitations. Note that only the MIV method resulted in the same ground-motion scaling factors, and therefore the same scaled records, for all four test specimens. The other scaling methods produced different scaling factors depending on the properties (e.g., fundamental period, T_1) of each structure. As discussed later in the paper, this is a practical advantage of the MIV method.

4 Test structures

Figure 2 depicts the 6-story 1-bay frame structure used in the shake-table tests. Center-to-center span length of 762 mm and story height of 432 mm were selected to achieve a length-scale of, approximately, $S_L = 1/10$ (i.e., specimen dimensions were approximately 1/10th of those from a full scale structure). In addition to this length scale, a time-scale of $S_T = 1/3$ was used to conduct the shake-table tests (i.e., the time domain of each record was scaled by a factor of 1/3; the S_a spectra in Fig. 1 include this time-scale factor). The values for $S_L = 1/10$ and $S_T = 1/3$ were selected to result in test specimens with fundamental periods and lateral strengths appropriate for a six-story building structure, also considering the physical capabilities of the shake-table (specimen size and payload limitations). The fundamental periods of the specimens were varied by varying the amount of superimposed mass at each floor level of the frame. The lateral strengths of the structures were varied by varying the moment strengths of the nonlinear beam-column connections. These variations resulted in the following four specimen configurations:

- Frame NL2R2—Structure with linear-elastic fundamental period of $T_1 = 0.22$ s and lateral strength of 1/2 of the linear-elastic base shear demand (to represent a response modification factor of $R = 2$) from the median 5%-damped S_a spectrum for the full suite of 39 unscaled records (considered as an "unbiased" design spectrum as discussed later).
- Frame NL2R4—Structure with linear-elastic fundamental period of $T_1 = 0.22$ s and lateral strength of 1/4 ($R = 4$) of the linear-elastic base shear demand from the median 5%-damped S_a spectrum for the 39 unscaled records.

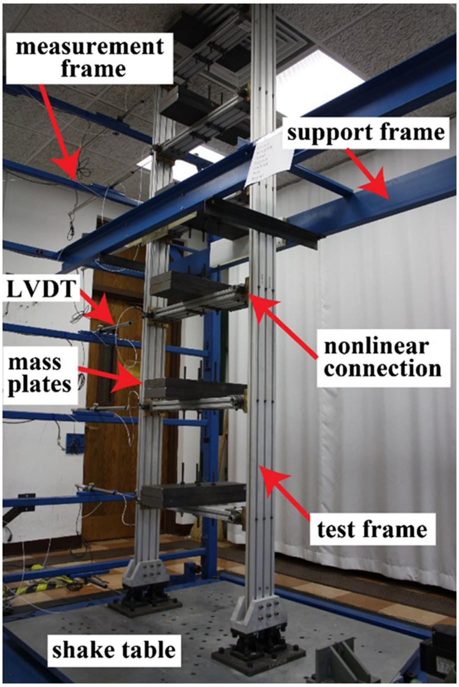

Fig. 2 6-story 1-bay frame test specimen with nonlinear beam-column connections, shown in Fig. 3 with more detail [adopted from O'Donnell et al. (2013b)]

- Frame NL4R2—Structure with linear-elastic fundamental period of $T_1 = 0.27$ s and lateral strength of 1/2 ($R = 2$) of the linear-elastic base shear demand from the median 5%-damped S_a spectrum for the 39 unscaled records.
- Frame NL4R4—Structure with linear-elastic fundamental period of $T_1 = 0.27$ s and lateral strength of 1/4 ($R = 4$) of the linear-elastic base shear demand from the median 5%-damped S_a spectrum for the 39 unscaled records.

The specimens with $T_1 = 0.22$ s (Frames NL2R2 and NL2R4) were configured with two superimposed mass plates at each floor and one plate at the roof, whereas the specimens with $T_1 = 0.27$ s (Frames NL4R2 and NL4R4) were configured with four mass plates at each floor and one plate at the roof. The weight of each superimposed plate was 21 kg, while the self-weight of the frame without any superimposed plates was 95 kg. The maximum number of superimposed mass plates (i.e., four plates at each floor) was limited by the payload capacity of the shake-table, while the minimum number of superimposed mass plates (i.e., two plates at each floor) was limited to ensure that the dynamic response of the structure was governed by lumped masses at the floor and roof levels rather than distributed masses from the self-weight of the frame. The linear-elastic fundamental period, T_1 of each specimen was determined by measuring the response of the structure to a long-duration small-amplitude white-noise base excitation. Due to the aforementioned limitations in the maximum and minimum number of superimposed mass plates, the difference between the fundamental periods of the test specimens was small (approximately 23%). Using the $S_T = 1/3$ time-scale, the measured specimen fundamental periods of $T_1 = 0.22$ and 0.27 s corresponded to full-scale periods of $T_1 = 0.66$ and 0.82 s, respectively. The measured second mode periods were $T_2 = 0.08$ s for Frames NL2R2 and NL2R4, and $T_2 = 0.09$ s for Frames NL4R2 and NL4R4. The linear-elastic damping ratio corresponding to the fundamental vibration mode of the structures was measured as 0.78% (same for all four frames) by applying the half-power bandwidth method to the white-noise base excitation response. From modal analysis, it was determined that both superimposed mass configurations resulted in similar modal mass participation factors, which were 87 and 9% for the first (fundamental) and second modes of vibration, respectively.

The beam and column members of the frame specimen were fabricated from extruded aluminum 6105-T5 alloy with a yield strength of 241 MN/m^2 to result in stiffness appropriate with the scale model and strength adequate to prevent yielding (O'Donnell et al. 2013a, 2015). The column bases were constructed with pinned connections. A tight-tolerance greased steel pin was used through each eye-bracket-to-clevis column base connection to reduce friction while mitigating backlash effects. To achieve a nonlinear but reusable structure, a nonlinear beam-column connection utilizing sliding friction interfaces was used at each beam end as shown in Fig. 3. This connection allowed the structures to demonstrate nonlinearity, inelastic energy dissipation, and permanent displacement, while still making it possible to loosen the connections and bring the structure back to its original condition after each earthquake.

As described in O'Donnell et al. (2015), a total of 12 identical beam-column connections were manufactured. To quantify the repeatability of the connection moment strength and nonlinear behavior, and to calibrate the relationship between the applied clamping torque and the connection strength, a series of pseudo-static reversed-cyclic tests as well as dynamic tests were conducted on each connection. These tests showed that the connections initially underwent a range of "stiffening" under repeated testing, but ultimately stabilized to provide a predictable nonlinear moment-rotation behavior. The resulting calibration data (after stabilization) was used to quantify the variability in the connection strength (for a

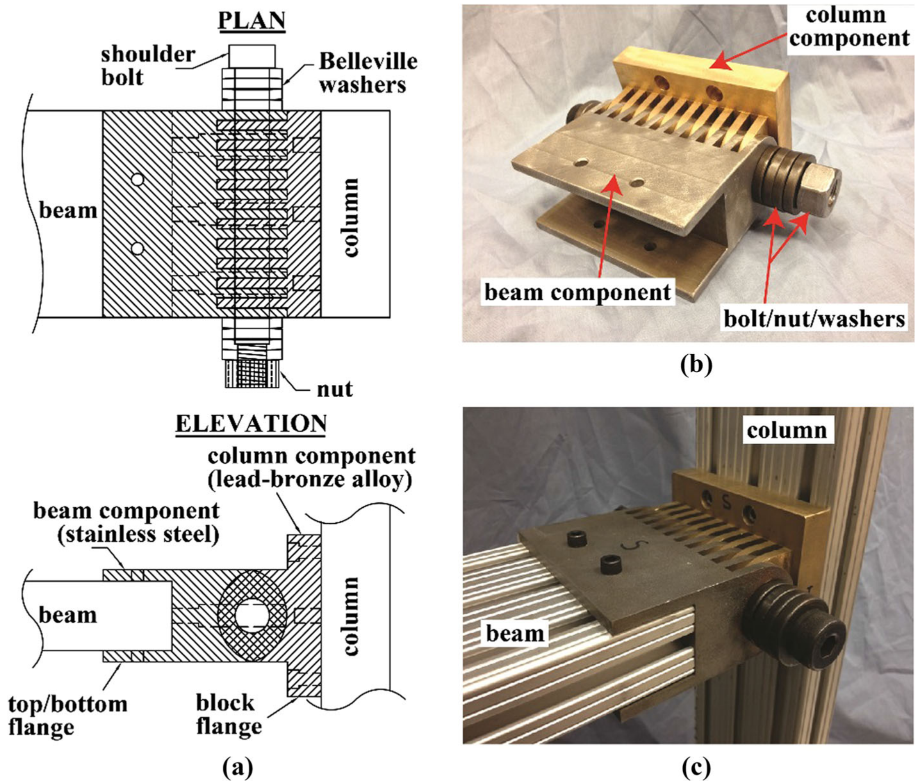

Fig. 3 Nonlinear beam-column connection design used to achieve repeatable nonlinear behavior in the frame specimens [adapted from O'Donnell et al. (2013b)]: **a** schematic; **b** photograph; **c** as assembled

specified clamping torque) and guide the placement of the 12 connections in the frame specimen. As can be seen from the dashed lines in Fig. 4 depicting a band of ± 1 standard deviation, σ from the fit line, each connection demonstrated a different level of uncertainty in its clamping torque, T_a to moment strength, M_{cm} relationship despite the fact that all 12 connections were fabricated and tested using the same process. The connections with lower standard deviation were placed in the lower floors and those with larger standard deviation were placed in the upper floors of the specimen to minimize the variability in the nonlinear behavior of the overall frame. The left–right and top-to-bottom ordering of the connection calibration plots in Fig. 4 illustrates how the connections were ultimately distributed within the frame; this distribution was kept the same in all shake-table tests of all four frame configurations. More information on the nonlinear beam-column connections and their testing can be found in O'Donnell et al. (2015).

To determine the design base shear demands, V_{bd} of the four frame specimens, first, the linear-elastic base shear demand (corresponding to $R = 1$) for each structure was calculated by multiplying the total mass with the median 5%-damped S_a spectrum for the full suite of 39 unscaled records at the measured fundamental period, T_1. Then, the linear-elastic base shear demands [see values given in O'Donnell et al. (2013b)] were divided by the response modification factors of $R = 2$ and $R = 4$ to determine V_{bd} representing

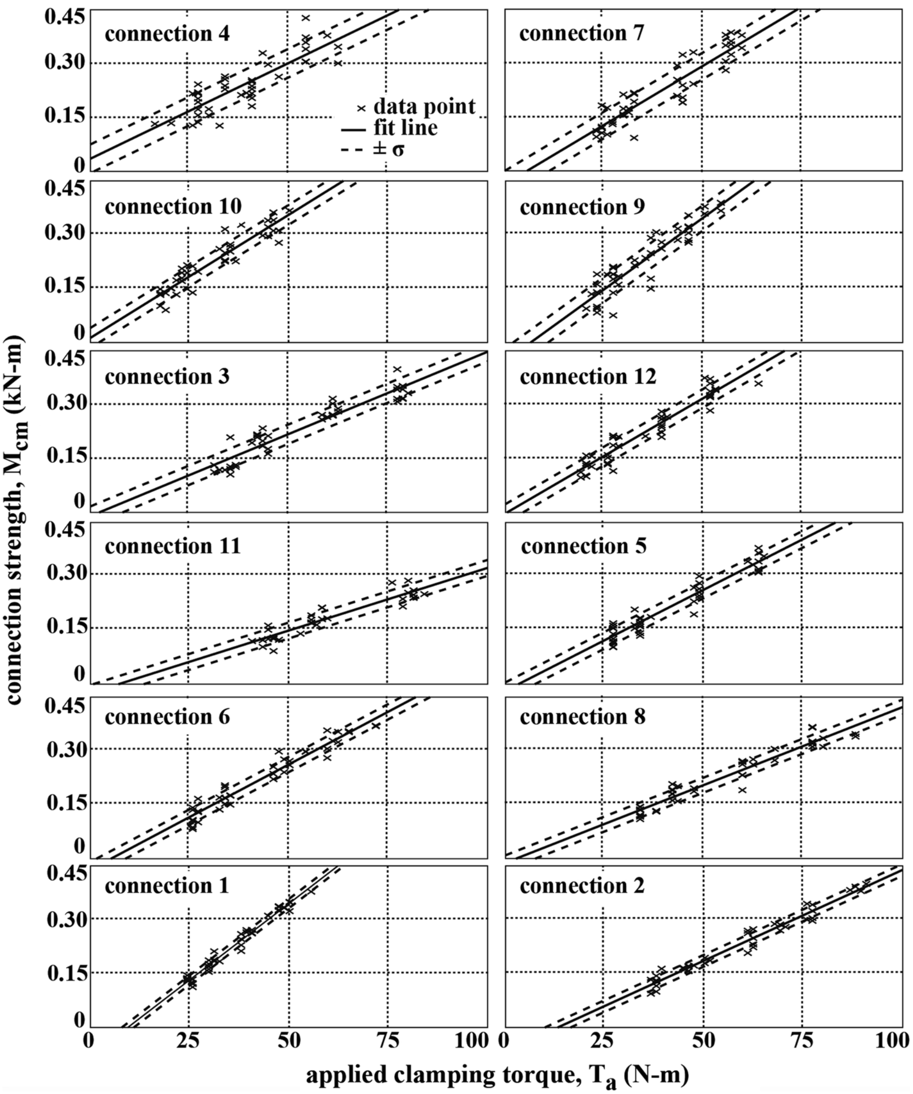

Fig. 4 Stable T_a versus M_{cm} calibration data set, depicting distribution of connections within each frame specimen

different degrees of nonlinearity ($R = 4$ representing a structure with smaller strength and greater nonlinearity). As described in O'Donnell et al. (2013b), the V_{bd} values calculated using the 5%-damped median S_a spectrum would correspond to greater R factors based on the 0.78%-damped median S_a spectrum (for the measured damping ratio of $\xi = 0.78\%$).

To result in test specimens with base shear strengths that closely satisfy V_{bd}, a series of monotonic and reversed-cyclic pushover tests were conducted on frame configurations with different moment strengths, M_{cm}, for the nonlinear beam-column connections (O'Donnell et al. 2013b). As described in O'Donnell et al. (2013a), these tests were conducted by holding the 4th floor of the frame stationary while slowly displacing the base

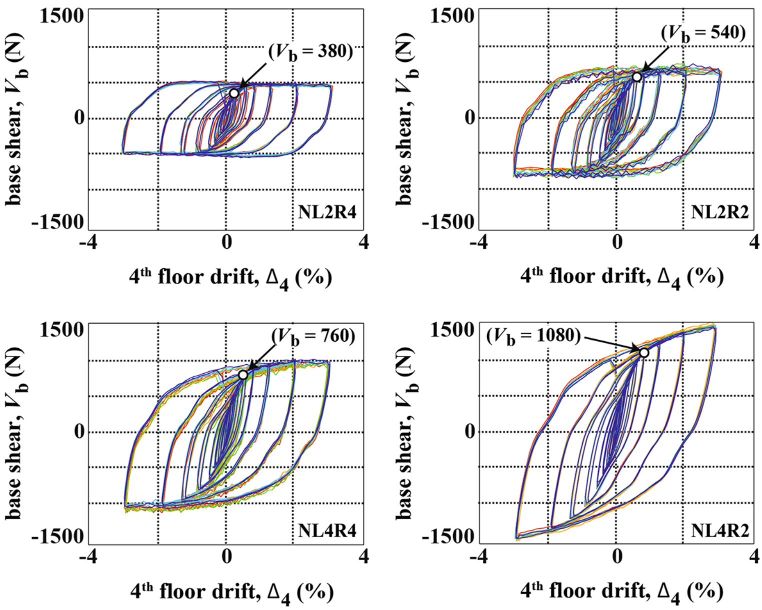

Fig. 5 Reversed-cyclic V_b–Δ_4 behaviors from five repeated tests for the four frame configurations (*different lines* in each plot depict five repeated test results for one frame configuration), showing that the measured lateral stiffness, strength, and nonlinear energy-dissipating characteristics exhibited excellent repeatability [adapted from O'Donnell et al. (2013b)]

using the shake-table. For each tested configuration, M_{cm} for all 12 connections at the floor and roof levels were kept constant. Between successive tests, each nonlinear connection was loosened, the structure brought back to vertical, and the connections re-tightened to the calibrated torque, T_a for the desired M_{cm}.

As an important requirement, while each frame configuration (with $R = 2$ or 4) was designed to undergo nonlinear hysteretic behavior during repeated dynamic testing under a large number of ground-motion records, the properties (i.e., lateral stiffness, strength, energy dissipation, period, damping) of the structure were required to remain similar from test to test. To demonstrate this requirement for static properties, Fig. 5 shows the base shear, V_b versus 4th floor drift, Δ_4 behavior of the four frame configurations under five repeated reversed-cyclic pushover tests. The tests were conducted in a non-sequential manner to result in the largest extent of variability possible. Five hysteresis curves are plotted in each graph, designating a different test of the structure and showing that the measured lateral stiffness, strength, and nonlinear energy-dissipating characteristics exhibited excellent repeatability. It can also be seen from these plots that the transition from the linear-elastic to post-yield behavior of the structures did not occur at a distinct yield point. Thus, the design base shear strength was determined at a characteristic yield point (○ markers in Fig. 5) by dividing the maximum base shear strength attained during the reversed-cyclic tests with an assumed over-strength factor of 1.4 (O'Donnell et al. 2013b).

The repeatability of the structures under dynamic loading is demonstrated in Fig. 6, which shows the roof drift, Δ time-history responses from five repeated shake-table tests (conducted in a non-sequential manner) under four different input ground-motions,

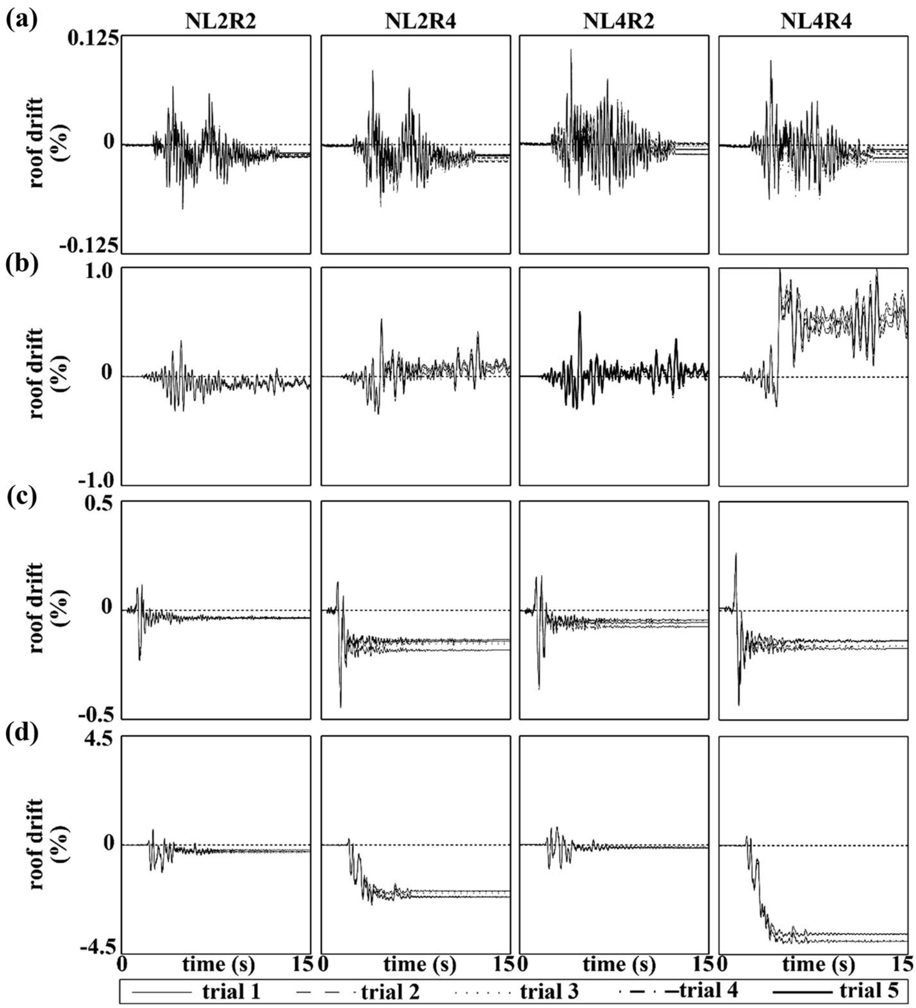

Fig. 6 Repeatability of dynamic roof drift response from five shake-table tests for the four frame configurations (*different lines* in each plot depict five repeated shake-table test results for one frame configuration) subjected to ground-motion records: **a** 1059-N; **b** FKS090; **c** GIL067; **d** KJM000 (see Table 1 for details of records)

resulting in a total of 80 tests for the four frames (the different lines in each plot depict the different shake-table test trials of the same frame configuration). Similar to the static test results in Fig. 5, between consecutive shake-table tests, each beam-column connection was loosened, the structure brought back to plumb, and the connections re-tightened to achieve the desired moment strength. The results indicate very good test-to-test consistency in the nonlinear dynamic roof drift response-history behaviors of the frames under the four ground-motions.

A more detailed evaluation of the dynamic response repeatability of the four frame configurations is discussed in O'Donnell et al. (2015), where the peak roof drift as well as the inter-story drift demands are investigated from repeated shake-table tests under a larger ensemble of ground-motion records. While the repeated test-to-test variability in the dynamic response of the structures under some of the ground-motions was larger (especially when considering the inter-story drift demands), the variability in the median demands from a suite of records was low, even for small subset suites of only 3 ground-motions. This finding validated the use of the nonlinear frame specimens for the ground-motion scaling study described herein, which focuses on median demands.

5 Effects of ground-motion scaling

5.1 Full suite results

During each shake-table test, close-to-simultaneous measurements (at 200 samples per second) of the floor and roof lateral displacements of the test frame as well as the displacements of the shake-table were measured using seven linear variable differential transformers. The resulting peak roof drift, Δ demands (i.e., peak roof displacement, D divided by the height from the column base pins) from the five suites of 36 ground-motions for each of the four structures are plotted in Fig. 7 against $S_a(T_1)$ (left) and MIV (right). It is clear from the large dispersion in the Δ demands that if only the maximum (in absolute value) demand from a small subset of records is used in design (for example, ASCE 7–10 allows suites with 3 records only), then the design outcome (i.e., over-design, under-design, satisfactory) can be drastically altered depending on the records selected, thus diminishing engineering confidence. As may be expected, all of the four scaling methods resulted in reduced dispersion in the peak drift demands of the structures when compared to the unscaled suite. A good correlation can be seen between Δ and MIV, indicating that the MIV scaling method may be effective in reducing the dispersion in the Δ demands.

The median [geometric mean; as described in Cornell et al. (2002)] of the peak roof drift demands (in absolute value) from the 36 unscaled records was taken as the "benchmark" median demand, $\hat{\Delta}_b$—regarded as the "true" representative demand of the site-specific seismic hazard—for each test frame. The "accuracy" of the scaling methods was quantified using the peak roof drift ratio, $r\left(\hat{\Delta}\right) = \hat{\Delta}/\hat{\Delta}_b$, where $\hat{\Delta}$ is the median peak roof drift demand from each scaled ground-motion suite. The error in preserving the benchmark median demand was calculated for each scaling method as $E\left(\hat{\Delta}\right) = r\left(\hat{\Delta}\right) - 1$. Table 2 shows the benchmark median peak roof drift demands, $\hat{\Delta}_b$ from the unscaled suites, as well as the errors, $E\left(\hat{\Delta}\right)$ in the median peak roof drift demands from the scaled suites for each structure.

As depicted in Fig. 8a, $E\left(\hat{\Delta}\right)$ quantifies whether a scaling method is more likely to underestimate (negative value) or overestimate (positive value) the benchmark median demand. Additionally, the coefficient of variation $COV(\Delta)$ of the peak roof drift demands for each structure under each ground-motion suite is shown in Fig. 8b and listed in Table 2. The COV, defined as the ratio between the sample standard deviation and the sample mean, is used to assess the effectiveness (i.e., "efficiency") of the scaling methods in reducing the dispersion in the peak roof drift demands.

With regard to minimizing the dispersion in the peak roof drift demands [i.e., smallest $COV(\Delta)$ values], the MIV scaling method performed the best, followed by the MPS

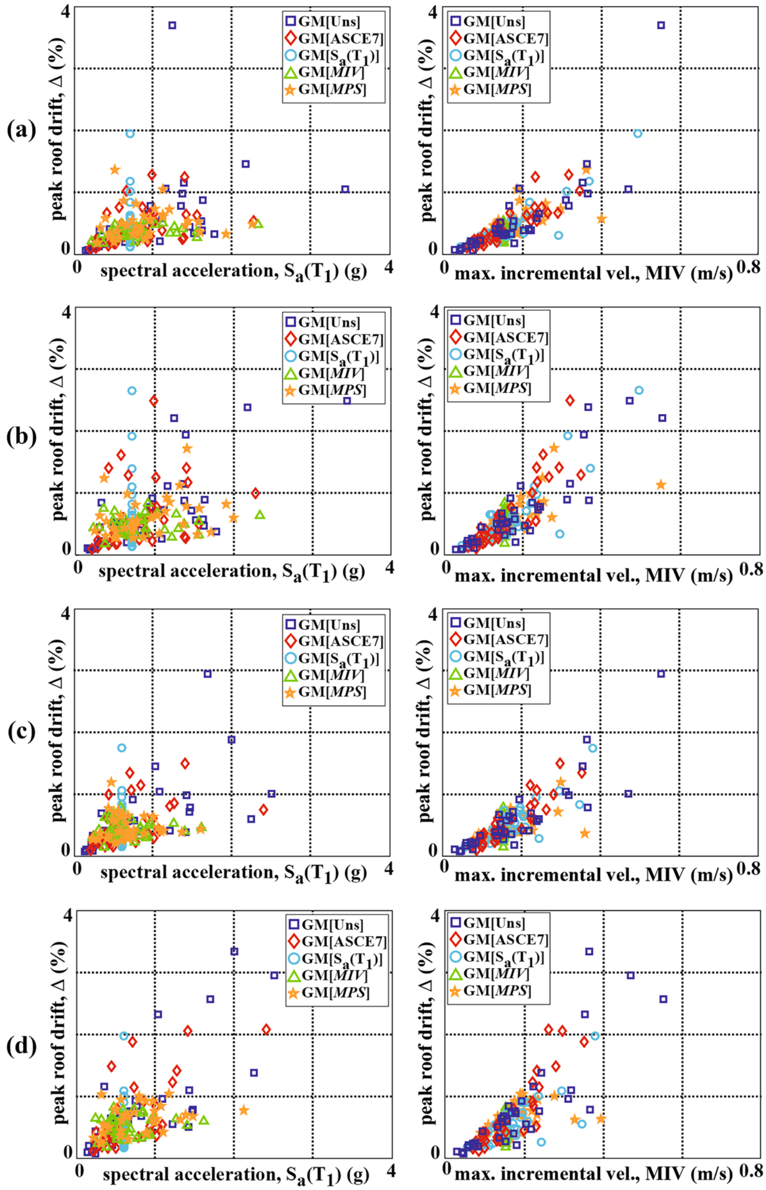

Fig. 7 Full suite results for peak roof drift, Δ demand [adopted from O'Donnell et al. (2013b)], showing better correlation of Δ with *MIV* than with $S_a(T_1)$: **a** Frame NL2R2; **b** Frame NL2R4; **c** Frame NL4R2; **d** Frame NL4R4

method, for all of the cases studied. The dispersion in Δ remained relatively constant between the four structures when using the MIV scaling method, whereas the dispersion in Δ showed greater variability between the structures when using the other scaling methods. With respect to accuracy as quantified by $E\left(\hat{\Delta}\right)$, the MIV method performed better than the other methods for most of the cases investigated (as can be seen from the bold cells in

Table 2 Full suite results for peak roof drift, Δ

Frame	GM[Uns]		GM[ASCE7]		GM[$S_a(T_1)$]		GM[MIV]		GM[MPS]	
	$\hat{\Delta}_b$ (%)	$COV(\Delta)$	$E(\hat{\Delta})$	$COV(\Delta)$	$E(\hat{\Delta})$	$COV(\Delta)$	$E(\hat{\Delta})$	$COV(\Delta)$	$E(\hat{\Delta})$	$COV(\Delta)$
NL2R2	0.37	1.14	−0.04	0.69	**−0.03**	0.80	−0.06	**0.27**	0.24	0.48
NL2R4	0.48	0.91	−0.07	0.87	−0.10	0.91	**−0.04**	**0.31**	0.15	0.51
NL4R2	0.43	0.94	−0.05	0.70	−0.03	0.65	−0.02	**0.32**	**0.01**	0.43
NL4R4	0.53	1.00	−0.08	0.83	−0.13	0.64	**−0.06**	**0.32**	0.13	0.36

GM[Uns], unscaled ground-motion suite; GM[ASCE7], ground-motion suite scaled based on ASCE 7; GM[$S_a(T_1)$], ground-motion suite scaled based on $S_a(T_1)$; GM[MIV], ground-motion suite scaled based on MIV; GM[MPS], ground-motion suite scaled based on MPS method; *COV*, coefficient of variation

Bold cells represent smallest (magnitude) $E(\hat{\Delta})$ and $COV(\Delta)$ for each frame

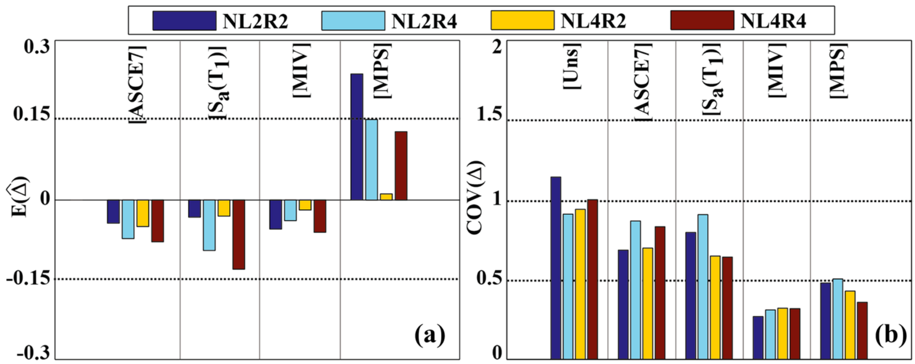

Fig. 8 Full suite results for peak roof drift, Δ, showing better overall performance of the MIV scaling method than the other methods considered: **a** error, $E(\hat{\Delta})$; **b** dispersion, $COV(\Delta)$

Table 2), only performing second best in accuracy for Frames NL2R2 and NL4R2 for which the $S_a(T_1)$ and MPS scaling methods performed better, respectively. This means that the MIV scaling method was better when used for the specimens with $R = 4$ than for the specimens with $R = 2$, thus pointing to improved accuracy of the MIV method as the nonlinearity of the structure is increased (i.e., greater R). As stated in Kurama and Farrow (2003), this improvement with greater R may be because the MIV method is able to better capture the longer-period characteristics of the ground-motions, which tend to excite nonlinear structures as they undergo period elongation. An evaluation of the suitability of the MIV scaling method for short period structures can be found in O'Donnell et al. (2013a), which shows significantly increased dispersion in the drift demands for a 1-story linear-elastic structure. The results in Fig. 8a also show the potential merits of the MPS method as it was the only method that resulted in positive $E(\hat{\Delta})$, thus pointing to safer (conservative) but potentially not as economical designs.

The $COV(\Delta)$ values in Table 2 for the four experimental frame specimens subjected to the GM[MIV] suite are similar to the numerical analysis results for two other frame structures evaluated in Kurama and Farrow (2003). However, as an important observation, the $COV(\Delta)$

values in Table 2 for the GM[$S_a(T_1)$] suites are significantly greater than the typical dispersion in the displacement demands obtained from previous numerical studies (e.g., Shome and Cornell 1998; Shome et al. 1998; Kennedy et al. 1984; Mehanny 1999; Alavi and Krawinkler 2000; Kurama and Farrow 2003). It has been reported that the dispersion from the $S_a(T_1)$ scaling method can be reduced by scaling at higher levels of damping (Shome and Cornell 1998; Kennedy et al. 1984). To evaluate the effect of the low level of measured inherent damping ($\xi = 0.78\%$) that was used to determine the scaling factors for the GM[$S_a(T_1)$] suite in the current experimental study, a numerical extension of the work was conducted. The numerical model was developed using the OpenSees structural analysis program (Mazzoni et al. 2011) based on the measured properties of the test specimens (e.g., measured period, lateral strength, energy dissipation), by outfitting a previous linear-elastic numerical model of the structure (O'Donnell et al. 2013a) with nonlinear zero-length rotational spring elements that emulated the measured behavior of the beam-column connections. In addition to the original ground motion scaling factors generated using $\xi = 0.78\%$, new scaling factors were determined from response spectra at $\xi = 5$, 10, and 20%. The damping ratio of $\xi = 5\%$ was selected because this is the level that most researchers have used in previous numerical studies. The damping ratios of $\xi = 10$ and 20% were selected to evaluate the range of the effect of this parameter.

Nonlinear dynamic RHAs of the OpenSees models under the four GM[$S_a(T_1)$] suites (scaled based on the four assumed levels of damping) were then conducted. The linear-elastic damping ratio of the nonlinear models in these dynamic analyses was equal to the measured inherent damping of $\xi = 0.78\%$ for the test specimens. The dispersion, $COV(\Delta)$ in the numerical peak roof drift demands are shown in Fig. 9a and the corresponding median peak roof drift demands, $\hat{\Delta}$ are shown in Fig. 9b. The $COV(\Delta)$ values demonstrate that ground motion scaling factors determined using higher damping resulted in significantly reduced dispersion [$COV(\Delta)$ dropped to the 0.36–0.74 range for scaling based on $\xi = 5\%$, 0.33–0.67 range for scaling based on $\xi = 10\%$, and 0.18–0.50 range for scaling based on $\xi = 20\%$]. The median demands, $\hat{\Delta}$ were not significantly affected by the amount of damping used to determine the scaling factors. These trends and reduced dispersion levels are consistent with previous relevant numerical studies (e.g., Shome and Cornell 1998). Only when a very high level of damping ($\xi = 10$ to 20%) was used to determine the scaling factors, then the dispersion values from the $S_a(T_1)$ scaling method dropped down to

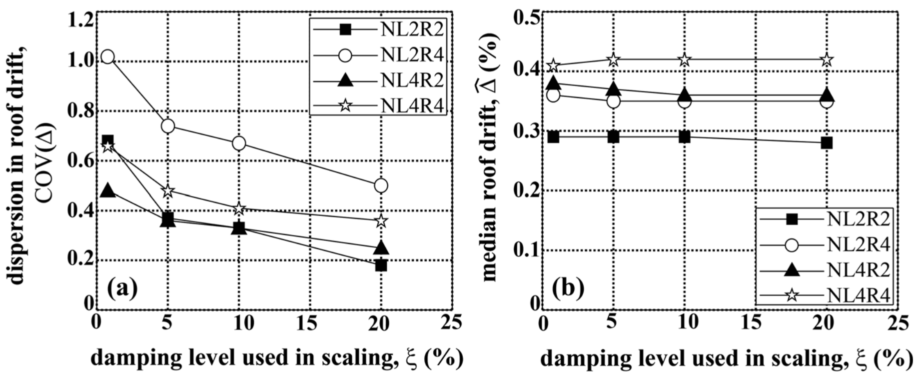

Fig. 9 Nonlinear response history analysis results using $S_a(T_1)$-suites scaled at higher-levels of damping, showing that $COV(\Delta)$ decreases significantly when using highly-damped ground-motion response spectra: **a** dispersion in peak roof drift, $COV(\Delta)$; **b** median peak roof drift, $\hat{\Delta}$

levels similar to those from the MIV method. This important characteristic for the $S_a(T_1)$ scaling method has been somewhat "lost" in the more recent literature, where $\xi = 5\%$ has been typically used both in determining the scaling factors and in conducting the nonlinear dynamic analyses. For this scaling method to be effective, the scaling factors must be determined using highly-damped ground-motion response spectra. Similar trends are likely valid for the ASCE 7 scaling method as well; however, this was not investigated in the current research. Note that probabilistic seismic hazard analysis (PSHA) often results in 5%-damped uniform hazard spectra, which can be scaled to higher damping values by means of conversion factors (e.g., Rezaeian et al. 2014).

Going back to the experimental study, the accuracy and efficiency of the scaling methods were also evaluated with regard to the peak inter-story drift demand, δ, in each story along the height of each structure. Note that this evaluation differs from that in O'Donnell et al. (2013b), which conducted comparisons based on the maximum-magnitude inter-story drift over the height of each structure (i.e., a single value of inter-story drift demand was considered from the response to each record, regardless of the story). In the current paper, accuracy is quantified using the peak inter-story drift ratio, $r\left(\hat{\delta}\right)$ and the corresponding error, $E\left(\hat{\delta}\right) = r\left(\hat{\delta}\right) - 1$, with $r\left(\hat{\delta}\right)$ calculated as the ratio between the median peak inter-story drift demand, $\hat{\delta}$ (in a given story) from each scaled ground-motion suite and the benchmark demand, $\hat{\delta}_b$ (see Table 3) defined as the median peak inter-story drift demand (in the same story) from the unscaled suite of 36 ground-motions. For example, Fig. 10 shows the variation in $r\left(\hat{\delta}\right)$ over the height of a test frame. Similar to the peak roof drift demand, a $r\left(\hat{\delta}\right)$ ratio of 1.0 represents perfect accuracy where the median peak inter-story drift demand from the scaled ground-motion suite, $\hat{\delta}$ matches the corresponding benchmark demand from the unscaled suite, $\hat{\delta}_b$. A negative error translates to an underestimation of the median benchmark demand whereas a positive error means an overestimation of the median benchmark demand. In order to compare the different scaling methods, Fig. 11a and Table 4 show the largest magnitude error, $E\left(\hat{\delta}\right)$ (with associated sign) over the height of each structure.

The dispersion in the peak inter-story drift demands, $COV(\delta)$ in each story was also calculated for each suite of ground-motions and the largest dispersion over the height of each structure was again used for the comparisons in Fig. 11b and Table 4. Looking at the results, the MIV scaling method performed the best, again followed by the MPS method, in minimizing the dispersion in the peak inter-story drift demands of the four test structures. Out of the methods investigated, the $S_a(T_1)$ scaling method was the least reliable in reducing the dispersion, exhibiting $COV(\delta)$ values as large as 1.18. With regard to the error, $E\left(\hat{\delta}\right)$ in preserving the benchmark median peak inter-story drift demands, the MIV

Table 3 Benchmark median peak inter-story drift demands, $\hat{\delta}_b$

Story	NL2R2 (%)	NL2R4 (%)	NL4R2 (%)	NL4R4 (%)
1	0.80	0.80	0.90	0.88
2	0.72	0.72	0.64	0.70
3	0.41	0.53	0.52	0.61
4	0.33	0.50	0.36	0.50
5	0.30	0.40	0.28	0.46
6 (roof)	0.21	0.44	0.18	0.39

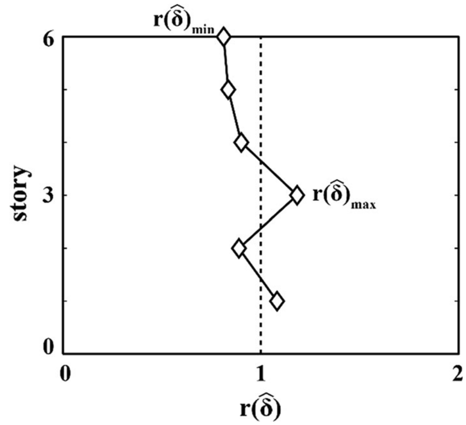

Fig. 10 Example variation of $r\left(\hat{\delta}\right)$ over the height of a test specimen; $r\left(\hat{\delta}\right) = 1.0$ represents perfect accuracy where $\hat{\delta}$ from a scaled ground-motion suite matches the benchmark demand, $\hat{\delta}_b$

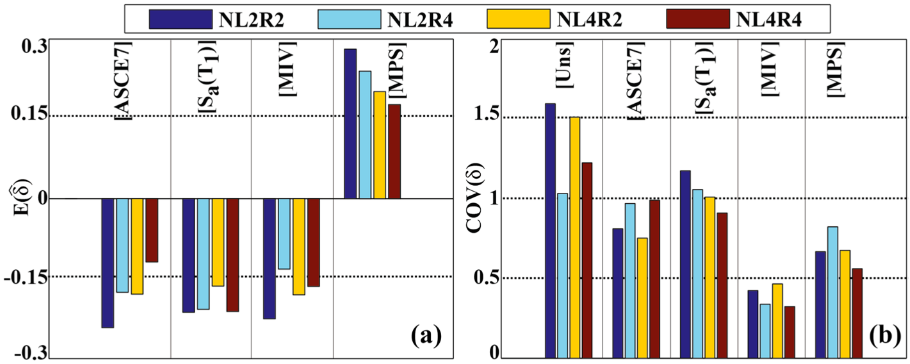

Fig. 11 Full suite results for peak inter-story drift, δ, showing differences between scaling methods in terms of: **a** largest magnitude error, $E\left(\hat{\delta}\right)$; **b** largest dispersion, $COV(\delta)$

Table 4 Full suite results for peak inter-story drift, δ (largest magnitude errors and dispersion over the height of each structure are reported)

Frame	GM[Uns]	GM[ASCE7]		GM[$S_a(T_1)$]		GM[MIV]		GM[MPS]	
	$COV(\delta)$	$E\left(\hat{\delta}\right)$	$COV(\delta)$	$E\left(\hat{\delta}\right)$	$COV(\delta)$	$E\left(\hat{\delta}\right)$	$COV(\delta)$	$E\left(\hat{\delta}\right)$	$COV(\delta)$
NL2R2	1.60	−0.24	0.81	**−0.21**	1.18	−0.23	**0.42**	0.28	0.67
NL2R4	1.03	−0.18	0.97	−0.21	1.06	**−0.13**	**0.34**	0.24	0.82
NL4R2	1.51	−0.18	0.75	**−0.16**	1.01	−0.18	**0.47**	0.20	0.68
NL4R4	1.22	**−0.12**	0.99	−0.21	0.91	−0.17	**0.33**	0.18	0.56

Bold cells represent smallest (in magnitude) $E\left(\hat{\delta}\right)$ and $COV(\delta)$ for each frame

method was outperformed by the $S_a(T_1)$ method for Frames NL2R2 and NL4R2, and by the ASCE 7 method for Frame NL4R4. The results again demonstrated that the MPS method was the only method that resulted in positive largest magnitude errors.

5.2 Subset suite results

In addition to evaluating the results from each full suite of 36 scaled ground-motion records, the experimental data was also analyzed through a subset simulation involving ground-motion bins with a smaller number of records consistent with the ground-motion suite sizes typically used by practitioners. This study quantified the ability of each scaling method to provide accurate estimates of the benchmark median peak roof drift and inter-story drift demands using a smaller set of ground-motion records (i.e., how close the median demands from a small subset of scaled ground-motions were to the corresponding median demands from the full unscaled suite of 36 ground-motions, which were considered as the benchmark). For this purpose, 9 subset ground-motion bins were constructed for each structure and scaling method, each bin containing the measured demands from 7 records out of the full set of 36 records (the use of 7 records is consistent with the ground-motion scaling requirements in the Nonlinear Seismic Response History Procedure of ASCE 7). The ground-motions for Bins 1–3 were chosen randomly from the full set, but Bins 4–6 were selected with a bias toward stronger ground-motions and Bins 7–9 were selected with a bias toward weaker ground-motions. To introduce this bias, the 36 unscaled ground-motions were sorted by ascending peak roof drift demand for each structure and the records were randomly selected either from below the median peak roof drift demand to introduce a weak bias or from above the median peak roof drift demand to introduce a strong bias. This procedure resulted in the selection of 9 bins of ground-motions for each of the four structures, where the ground-motions in each bin for a given structure were the same for all four scaling methods.

Similar to the full suite comparisons, the accuracy of each scaling method was quantified using the subset peak roof drift ratio, $r\left(\hat{\Delta}_s\right)$ and the corresponding error, $E\left(\hat{\Delta}_s\right) = r\left(\hat{\Delta}_s\right) - 1$, with $r\left(\hat{\Delta}_s\right)$ defined as the ratio between the median peak roof drift demand, $\hat{\Delta}_s$ from the ground-motions in each subset bin of 7 records and the benchmark demand, $\hat{\Delta}_b$ from the full unscaled suite of 36 records. Additionally, the subset dispersion was calculated as the $COV(\Delta_s)$ of the 7 peak roof drift demands in each ground-motion bin. Figure 12 shows the performance of the scaling methods with respect to $E\left(\hat{\Delta}_s\right)$ and $COV(\Delta_s)$. It is important that both $E\left(\hat{\Delta}_s\right)$ and $COV(\Delta_s)$ be considered in evaluating the scaling methods. For example, looking at the results for Frame NL4R2 in Fig. 12b, the $COV(\Delta_s)$ value for Bin 5 from the ASCE7-scaled suite is relatively small (indicating low dispersion in the roof drift demands). However, the magnitude of $E\left(\hat{\Delta}_s\right)$ for the same bin for NL4R2 in Fig. 12a is very large, indicating poor accuracy in the results.

To further analyze and condense the results, Table 5 shows the average and maximum values of the error magnitudes, $\left|E\left(\hat{\Delta}_s\right)\right|$ from the 9 analysis bins for each structure and scaling method. Similarly, Table 6 shows the average and maximum values for the dispersions, $COV(\Delta_s)$ from the 9 bins. While there was considerable variability between the different bins (Fig. 12), the results are consistent with the findings from the analysis of the full ground-motion suites that the MIV scaling method was more effective in minimizing bin dispersion, $COV(\Delta_s)$. The MIV method was also the most accurate (i.e., it resulted in the smallest average and maximum $\left|E\left(\hat{\Delta}_s\right)\right|$ values) for Frames NL2R4 and NL4R4. For Frames NL2R2 and NL4R2, the $S_a(T_1)$ and MPS methods, respectively, produced better

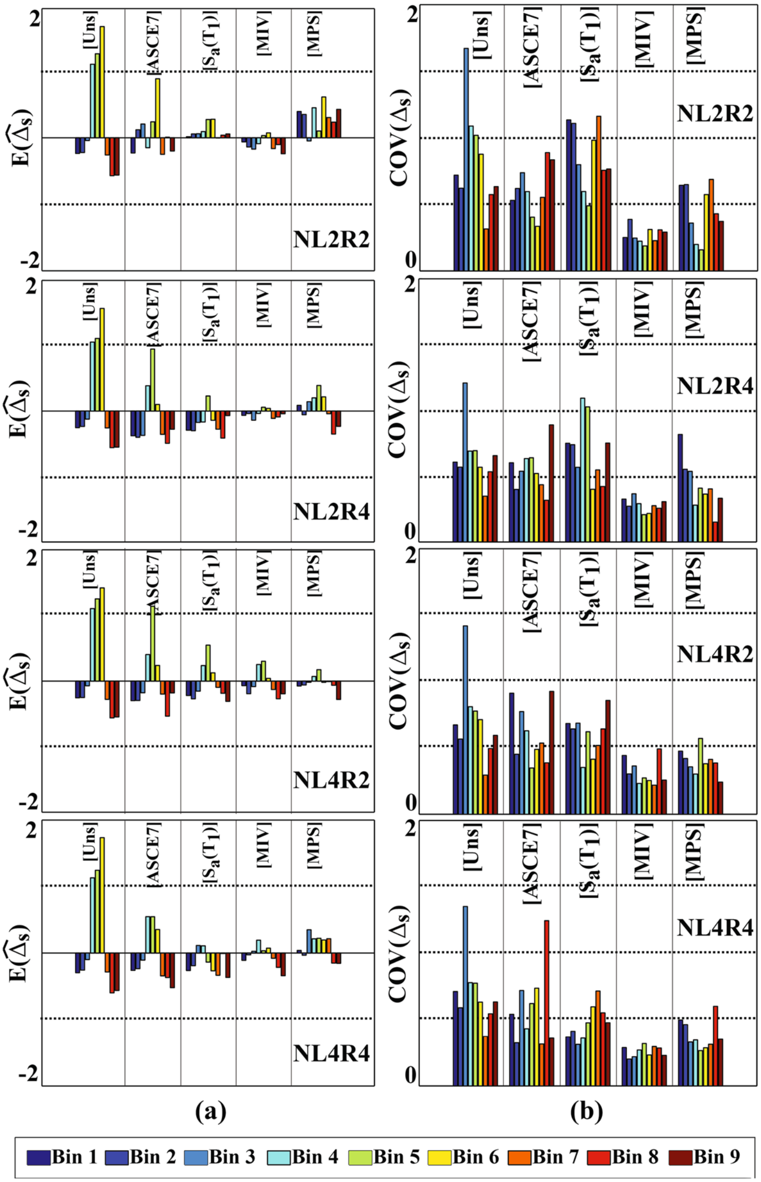

Fig. 12 Comparison of scaling methods when used with smaller subsets of ground-motion records in Bins 1–9, with respect to: **a** error in median peak roof drift, $E\left(\hat{\Delta}_s\right)$; and **b** dispersion in peak roof drift, $COV(\Delta_s)$

bin accuracy, indicating that the overall effectiveness of the MIV method was smaller for the specimens with smaller nonlinearity (i.e., smaller *R*) than those with larger nonlinearity (i.e., larger *R*).

Additionally, the scaling methods were evaluated using the peak inter-story drift ratio, $r\left(\hat{\delta}_s\right)$ and the corresponding error, $E\left(\hat{\delta}_s\right) = r\left(\hat{\delta}_s\right) - 1$ from the subset ground-motion

Table 5 Subset suite results for $\left|E\left(\hat{\Delta}_s\right)\right|$ (average and maximum values of error magnitudes in median peak roof drift are reported)

Frame	GM[Uns]		GM[ASCE7]		GM[$S_a(T_1)$]		GM[MIV]		GM[MPS]	
	Avg	Max	Avg	Max	Avg	Max	Avg	Max	Avg	Max
NL2R2	0.66	1.67	0.25	0.89	**0.10**	0.28	0.12	**0.24**	0.33	0.61
NL2R4	0.64	1.57	0.41	0.95	0.23	0.41	**0.07**	**0.14**	0.19	0.39
NL4R2	0.63	1.40	0.38	1.12	0.24	0.54	0.17	0.30	**0.08**	**0.28**
NL4R4	0.69	1.73	0.36	0.55	0.20	0.37	**0.12**	**0.34**	0.18	0.35

Bold cells represent smallest average and maximum $\left|E\left(\hat{\Delta}_s\right)\right|$ for each frame

Table 6 Subset suite results for dispersion in peak roof drift, $COV(\Delta_s)$ (average and maximum values of dispersion in peak roof drift are reported)

Frame	GM[Uns]		GM[ASCE7]		GM[$S_a(T_1)$]		GM[MIV]		GM[MPS]	
	Avg	Max	Avg	Max	Avg	Max	Avg	Max	Avg	Max
NL2R2	0.84	1.67	0.61	0.89	0.87	1.16	**0.27**	**0.39**	0.45	0.69
NL2R4	0.65	1.21	0.55	0.89	0.70	1.09	**0.28**	**0.37**	0.43	0.82
NL4R2	0.71	1.42	0.61	0.93	0.60	0.86	**0.32**	**0.49**	0.39	0.57
NL4R4	0.71	1.35	0.59	1.25	0.48	0.72	**0.26**	**0.32**	0.38	0.60

Bold cells represent smallest average and maximum $COV(\Delta_s)$ for each frame

suites, with $r\left(\hat{\delta}_s\right)$ defined as the ratio between the median peak inter-story drift demand, $\hat{\delta}_s$ (in a given story) from each subset bin of 7 records and the benchmark demand, $\hat{\delta}_b$ (in the same story) from the full unscaled suite of 36 records. The dispersion in the subset peak inter-story drift demands, $COV(\delta_s)$ was also calculated for each story. To compare the different scaling methods, Fig. 13 shows the largest magnitude error, $E\left(\hat{\delta}_s\right)$ (with associated sign) and the largest dispersion, $COV(\delta_s)$ in the peak inter-story drift demands over the height of each structure.

To further analyze the results, Table 7 shows the average and maximum values of the largest error magnitudes, $\left|E\left(\hat{\delta}_s\right)\right|$ (over structure height) from the 9 analysis bins for each structure and scaling method. Similarly, Table 8 shows the average and maximum values for the largest dispersion, $COV(\delta_s)$ (over structure height) from the 9 bins. The results again support the finding that the MIV scaling method was consistently more effective in minimizing the bin dispersion, $COV(\delta_s)$. In terms of the error magnitudes, $\left|E\left(\hat{\delta}_s\right)\right|$, the MIV method produced better results for Frames NL2R4 and NL4R4, but not for Frames NL2R2 and NL4R2 [the $S_a(T_1)$ and MPS methods produced smaller bin error magnitudes, $\left|E\left(\hat{\delta}_s\right)\right|$ for these frames, respectively]. These results again show that the effectiveness of the MIV method was better for the structures with greater nonlinearity.

The decreased dispersion in the peak seismic displacement demands using the MIV scaling method coupled with the fact that it can be implemented independent of the

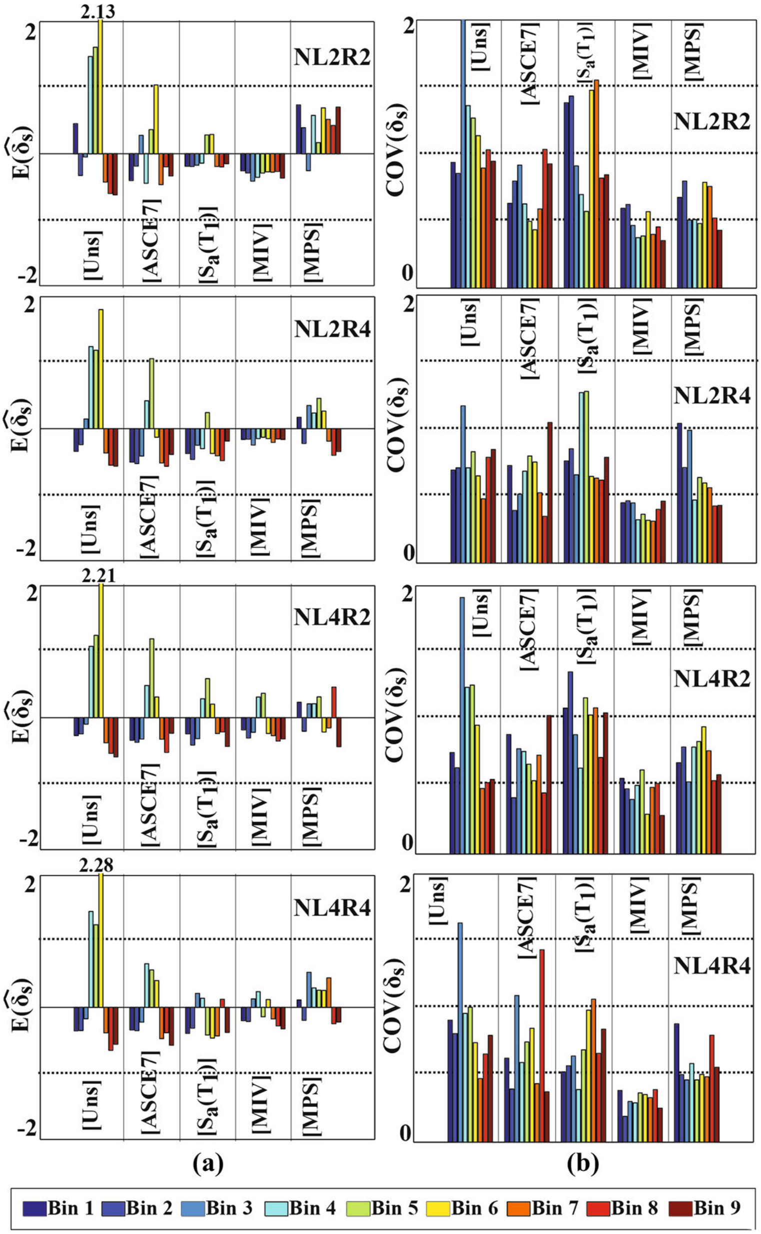

Fig. 13 Comparison of scaling methods when used with smaller subsets of ground-motion records in Bins 1–9, with respect to: **a** largest magnitude error (over structure height) in median peak inter-story drift, $E\left(\hat{\delta}_s\right)$; and **b** largest dispersion (over structure height) in peak inter-story drift, $COV(\delta_s)$

properties of the structure being analyzed are significant advantages for this scaling method. Any changes in the structure properties (e.g., fundamental period, T_1) during the design iterations would not require re-scaling of the selected ground-motions. Additionally, as shown in O'Donnell et al. (2013a), the effectiveness of scaling methods that depend on

Table 7 Subset suite results for largest error magnitude in median peak inter-story drift, $\left|E\left(\hat{\delta}_s\right)\right|$

Frame	GM[Uns]		GM[ASCE7]		GM[$S_a(T_1)$]		GM[MIV]		GM[MPS]	
	Avg	Max	Avg	Max	Avg	Max	Avg	Max	Avg	Max
NL2R2	0.85	2.13	0.41	1.02	**0.20**	**0.29**	0.31	0.41	0.49	0.73
NL2R4	0.71	1.78	0.50	1.04	0.34	0.48	**0.17**	**0.25**	0.29	0.45
NL4R2	0.73	2.21	0.45	1.18	0.32	0.58	0.28	**0.36**	**0.27**	0.46
NL4R4	0.82	2.28	0.44	0.65	0.32	0.46	**0.20**	**0.32**	0.28	0.52

Bold cells represent smallest average and maximum $\left|E\left(\hat{\delta}_s\right)\right|$ for each frame

Table 8 Subset suite results for largest dispersion in peak inter-story drift, $COV(\delta_s)$

Frame	GM[Uns]		GM[ASCE7]		GM[$S_a(T_1)$]		GM[MIV]		GM[MPS]	
	Avg	Max	Avg	Max	Avg	Max	Avg	Max	Avg	Max
NL2R2	1.16	2.03	0.72	1.03	1.08	1.55	**0.47**	**0.62**	0.61	0.80
NL2R4	0.77	1.17	0.64	1.05	0.84	1.28	**0.39**	**0.46**	0.65	1.04
NL4R2	0.93	1.91	0.70	1.03	1.00	1.36	**0.47**	**0.63**	0.72	0.95
NL4R4	0.89	1.63	0.73	1.44	0.71	1.07	**0.32**	**0.39**	0.58	0.88

Bold cells represent smallest average and maximum $COV(\delta_s)$ for each frame

the structure properties (e.g., the ASCE 7 and $S_a(T_1)$ methods require T_1 and the MPS method requires the nonlinear monotonic pushover behavior of the structure) can erode due to inaccuracies in the design estimation of these properties, potentially leading to poor estimation of the seismic demands.

The biggest disadvantage for the implementation of the MIV scaling method in current seismic design procedures is the lack of methods to estimate the mean annual frequency of exceedance of *MIV* and methods to estimate the attenuation of *MIV*. Thus, there is currently no method to determine the probability of exceedence of a certain *MIV* level at a given site, and therefore no method to determine a target *MIV* for design. Future research is needed in these areas before the MIV scaling method can be used in practice.

6 Summary and conclusions

This paper described an experimental evaluation of four ground-motion scaling methods [ASCE7, $S_a(T_1)$, MIV, and MPS] for use in nonlinear response history analysis in seismic design. These methods were evaluated on the basis of their ability to both minimize the dispersion and maximize the accuracy in the dynamic peak roof and inter-story drift demands of nonlinear building frame structures. A comprehensive database of 720 dynamic response histories was developed by subjecting four small-scale frame specimens to an unscaled suite of 36 ground-motions, and four suites of 36 ground-motions scaled according to the aforementioned scaling methods. The results were evaluated based on the dispersion in the peak roof drift and inter-story drift demands of the test frames, as well as the accuracy in the median peak drift demands as compared with the benchmark median peak drift demands from the unscaled suite of 36 records. Importantly, this evaluation also included a component by which the demands from unbiased and biased selections of smaller subsets of 7 ground-motions were evaluated for dispersion and accuracy as compared against the benchmark demands from the full suite of 36 unscaled ground-motions in order to simulate a more typical design-type scenario. The following main conclusions were drawn from the analysis of the data. Note that while these conclusions appeal attention to observed trends in the performance of the four scaling methods, they may be limited to the ground-motion records and structures that were considered within the context of this research investigation.

1. Results from the full scaled suites of 36 ground-motions showed that the MIV method consistently reduced the dispersion in the peak drift demands better than the other three scaling methods. The MIV method was also most effective in preserving the benchmark median drift demands for the test structures with greater nonlinearity; however, the accuracy of the method was somewhat reduced for the structures with smaller nonlinearity.
2. The large dispersion in the peak drift demands for the $S_a(T_1)$ method was because the scaling factors were determined based on the measured inherent damping of the test structures, which was very low. The median peak drift demands were not significantly affected by the amount of damping used to determine the scaling factors. Only when a very high damping ratio ($\xi = 10$–20%) was used to determine the scaling factors, did the dispersion from the $S_a(T_1)$ scaling method drop down to levels similar to those from the MIV method. Thus, it is concluded that for the $S_a(T_1)$ scaling method to be effective, the scaling factors must be determined using highly-damped response spectra. This important characteristic for the $S_a(T_1)$ method has been somewhat "lost" in the more recent literature, where $\xi = 5\%$ has been traditionally used both in determining the scaling factors and in conducting the nonlinear dynamic response history analyses.
3. The MPS scaling method was the second best method (after MIV) in reducing dispersion and was also the only method to overestimate the median demands with respect to the benchmark demands, thereby leading to more conservative (but less economical) designs. The MPS method depends on the nonlinear monotonic pushover behavior of the structure (which is often available prior to nonlinear dynamic response history analysis in practice), as well as the peak displacements of the resulting equivalent nonlinear single-degree-of-freedom model (which can be estimated from nonlinear dynamic response history analyses or by using approximate nonlinear displacement demand prediction relationships).
4. Analyses of the experimental data from smaller subsets of 7 ground-motion records instead of the full suites of 36 records generally supported the observations above.
5. Out of the four scaling methods, the MIV method was the only method that did not depend on the properties (e.g., period, lateral strength) of the structure, which is an important practical advantage.

7 Data and resources

The ground-motion records used in this study were obtained from the PEER ground-motion database at http://peer.berkeley.edu/ngawest2/databases/ (last accessed on January 5, 2015). The numerical models of the test specimens are available from the authors upon request. Further details of the experimental study, including time series of ground-motion sets and measured engineering demand parameters, are at http://www3.nd.edu/~seismic/Available_Data.html (last accessed on January 5, 2015).

Acknowledgements This research was funded by the National Science Foundation (NSF) under Grant No. CMMI 0928662. The support of former NSF Program Directors, Dr. K.I. Mehta and Dr. M.P. Singh, is gratefully acknowledged. The authors would like to thank Brad Aagaard (United States Geological Survey), Mahdi Ebrahimian (Kleinfelder, Inc.), and Neal S. Kwong (The Cooper Union) for their review and constructive comments on the paper. The authors would also like to acknowledge the following individuals for their guidance, through informal discussions, in formulating the research questions and the approaches to their investigation: Paulo Bazzurro, University Institute for Superior Studies; Sigmund Freeman, Wiss, Janney, Elstner Associates, Inc.; Vladimir Graizer, U.S. Nuclear Regulatory Commission; Farzad Naeim, John A. Martin and Associates, Inc.; and Thomas Sabol, Englekirk & Sabol Consulting Structural Engineers, Inc. Additionally, Bob St. Henry, NEFF Engineering, helped in the design and construction of the test specimens. The opinions, findings, and conclusions in the paper do not necessarily reflect the views of the organizations or individuals acknowledged above.

References

Alavi B, Krawinkler H (2000) Consideration of near-fault ground motion effects in seismic design. In: 12th world conference on earthquake engineering. Paper no. 2665, Auckland

American Society of Civil Engineers (ASCE) (2010) Minimum design loads for buildings and other structures. ASCE standard 7–10

Ay B, Akkar S (2014) Evaluation of a recently proposed record selection and scaling procedure for low-rise to mid-rise reinforced concrete buildings and its use for probabilistic risk assessment studies. Earthq Eng Struct Dyn 43(6):889–908

Chopra AK, Chinatanapakdee C (2004) Inelastic deformation ratios for design and evaluation of structures: single-degree-of-freedom bilinear systems. J Struct Eng 130(9):1309–1319

Cornell C, Jalayer F, Hamburger R, Foutch D (2002) Probabilistic basis for 2000 SAC federal emergency management agency steel moment frame guidelines. J Struct Eng 128(4):526–533

Haselton C (2009) Evaluation of ground motion selection and modification methods: predicting median interstory drift response of buildings. Pacific Earthquake Engineering Research (PEER) Center, California State University, Chico, CA

Kalkan E, Chopra AK (2009) Modal pushover-based ground motion scaling procedure for nonlinear response history analysis of structures. In: Proceedings of the structural engineering association of California, annual convention, San Diego

Kalkan E, Chopra A (2010a) Modal-pushover-based ground-motion scaling procedure. J Struct Eng 137(3):298–310

Kalkan E, Chopra A (2010b) Practical guidelines to select and scale earthquake records for nonlinear response history analysis of structures. US geological survey open-file report, 1068

Kalkan E, Chopra A (2012) Evaluation of modal pushover-based scaling of one component of ground motion: tall buildings. Earthq Spectra 28(4):1469–1493

Kalkan E, Kunnath SK (2006) Effects of fling-step and forward directivity on the seismic response of buildings. Earthq Spectra 22(2):367–390

Kalkan E, Kwong NS (2010) Documentation for assessment of modal pushover-based scaling procedure for nonlinear response history analysis of "ordinary standard" bridges, US. Geological survey open-file report no 2010-1328, p. 56

Kalkan E, Kwong NS (2012) Assessment of modal pushover-based scaling procedure for nonlinear response history analysis of "ordinary standard" bridges. J Bridge Eng 17(2):272–288

Kennedy R, Short S, Merz K, Tokarz F, Idriss I, Powers M, Sadigh K (1984) Engineering characterization of ground motion-task I: effects of characteristics of free-field motion on structural response. NUREG/CR-3805. US Regulatory Comm. Washington, DC

Kurama Y, Farrow K (2003) Ground motion scaling methods for different site conditions and structure characteristics. Earthq Eng Struct Dyn 32(15):2425–2450

Mazzoni S, McKenna F, Scott M, Fenves G (2011) Open system for earthquake engineering simulation: OpenSees command language manual. University of California, Berkeley. http://opensees.berkeley.edu/

Mehanny S (1999) Modeling and assessment of seismic performance of composite frames with reinforced concrete columns and steel beams. Ph.D. thesis, Civil and Environmental Engineering, Stanford, USA

Naeim F, Alimoradi A, Pezeshk S (2004) Selection and scaling of ground motion time histories for structural design using genetic algorithms. Earthq Spectra 20:413

Nau J, Hall W (1984) Scaling methods for earthquake response spectra. J Struct Eng 110(7):1533–1548

O'Donnell A, Kurama Y, Kalkan E, Taflanidis A, Beltsar A (2013a) Ground motion scaling methods for linear-elastic structures: an integrated experimental and analytical investigation. Earthq Eng Struct Dyn 42(9):1281–1300

O'Donnell A, Kurama Y, Kalkan E, Taflanidis A (2013b) Experimental evaluation of ground motion scaling methods for nonlinear analysis of structural systems. ASCE/SEI structures congress 2013, Pittsburgh, PA, 12 pp

O'Donnell A, Kurama Y, Taflanidis A, Kalkan E (2015) A nonlinear frame test structure with repeatable behavior for experimental dynamic response history investigation. J Earthq Eng. doi:10.1080/13632469.2015.1046571

Reyes JC, Chopra A (2012) Modal pushover-based scaling of two components of ground-motion records for nonlinear RHA of structures. Earthq Spectra 28(3):1243–1267

Reyes JC, Quintero O (2013) Modal pushover-based scaling of earthquake records for nonlinear analysis of single-story unsymmetric-plan buildings. Earthq Eng Struct Dyn 43(7):1005–1021

Reyes JC, Riaño AC, Kalkan E, Arango CM (2015) Extending modal pushover-based scaling (MPS) procedure for nonlinear response history analysis of multi-story unsymmetric-plan buildings. Eng Struct 88:125–137

Rezaeian S, Bozorgnia Y, Idriss IM, Campbell K, Abrahamson N, Silva W (2014) Damping scaling factors for elastic response spectra for shallow crustal earthquakes in active tectonic regions: 'Average' horizontal component. Earthq Spectra 30(2):939–963

Shome N, Cornell C (1998) Normalization and scaling accelerograms for nonlinear structural analysis. In: Sixth US national conference on earthquake engineering, Seattle, WA

Shome N, Cornell C, Bazzurro P, Carballo J (1998) Earthquakes, records, and nonlinear responses. Earthq Spectra 14(3):469–500